

# Hyperbolic Plasmons and Topological Transitions Over Uniaxial Metasurfaces

J. Sebastian Gomez-Diaz, Mykhailo Tymchenko, and Andrea Alù\*

*Department of Electrical and Computer Engineering, The University of Texas at Austin,  
1616 Guadalupe Street, UTA 7.215, Austin, Texas 78701, USA*

(Received 9 February 2015; published 11 June 2015)

We explore the unusual electromagnetic response of ultrathin anisotropic  $\sigma$ -near-zero uniaxial metasurfaces, demonstrating extreme topological transitions—from closed elliptical to open hyperbolic—for surface plasmon propagation, associated with a dramatic tailoring of the local density of states. The proposed metasurfaces may be implemented using nanostructured graphene monolayers and open unprecedented venues for extreme light confinement and unusual propagation and guidance, combined with large tunability via electric bias.

DOI: 10.1103/PhysRevLett.114.233901

PACS numbers: 42.25.Bs, 73.20.Mf, 78.67.Pt

Hyperbolic materials [1–4] are uniaxial media with extreme anisotropy, whose effective permittivity changes sign as a function of the electric field polarization. Electromagnetic waves traveling in these media follow a hyperbolic dispersion, supporting propagation of extremely confined waves that would be evanescent in conventional media. The advent of metamaterials [5] and recent advances in nanofabrication and material characterization have provided a well-established platform to propose and experimentally realize hyperbolic metamaterials (HMTMs) [4–8] across the frequency spectrum. The exciting properties of HMTMs include strong and broadband enhancement of spontaneous emission rate (SER) of an emitter located within or near the interface of such materials [4,9,10], large absorption [4], subdiffraction light localization [4], negative refraction [4], and canalization of the incoming energy [11,12].

The complex fabrication of bulk metamaterials, however, has significantly hindered the impact of this technology, especially for optical metamaterials, and volumetric effects may be detrimental for the associated losses. In order to circumvent these issues, the concept of *metasurfaces* (MTSs) [13–15], i.e., planarized ultrathin metamaterials, has been introduced, which solves many of the present challenges of metamaterials, and allows integration with planarized systems compatible with integrated circuits. This may be particularly relevant for many of the proposed applications of HMTMs, for which propagation in the bulk of the material may be undesirable. For instance, large enhancement in Purcell emission from small fluorophores placed on the HMTM interface may not be detectable once it couples to modes propagating in the bulk of the material, especially if losses are not negligible.

Recently, wave propagation and topological transitions in a 2D cut of a bulk hyperbolic transmission-line metamaterial have been demonstrated [16]. In addition, several works have proposed that the unusual response of hyperbolic materials may be translated into metasurfaces by

simply reducing their profile [14,17]. These approaches not only face similar fabrication challenges, but they also raise important theoretical questions, as it may be ambiguous to assign bulk material properties to ultrathin structures. Also, simply thinning down HMTMs misses an important portion of the rich physics peculiar of optical MTSs, associated with their reduced dimensionality and the propagation of surface plasmons able to interact with the surrounding media. In this context, the area of graphene plasmonics [18–20] has recently emerged as an ideal platform for strong-light matter interactions over 2D surfaces, offering significant advantages over more traditional plasmonic platforms in terms of electronic tunability, large field confinement, and integrability, which have triggered significant interest and a plethora of exciting applications [21–24]. These properties, as an example relevant to hyperbolic propagation, were recently exploited in Ref. [25] to put forward an extremely anisotropic planar hyperlens obtained by modulating the conductivity of a uniform 2D graphene sheet.

Here, we introduce the concept of ultrathin hyperbolic and extremely anisotropic  $\sigma$ -near-zero metasurfaces. Their inherently 2D nature allows a straightforward modeling using a uniaxial surface conductivity tensor, able to take into account their reduced dimensionality while providing an ideal platform for their rigorous characterization. First, we derive and study the dispersion relation and extreme light confinement of plasmons supported by the proposed MTSs. Compared to wave propagation in usual hyperbolic bulk media, hyperbolic plasmons possess evanescent fields in the direction perpendicular to the metasurface, thus allowing strong light-matter interactions while providing extreme field confinement. Then, we show that an array of densely packed graphene strips may implement any metasurface topology, ranging from elliptical to hyperbolic dispersion, and going through extremely anisotropic  $\sigma$ -near-zero conductivity. This structure—analyzed using an in-plane effective medium approach—demonstrates the possibility to realize HMTMs in a realistic configuration that

can be electrically reconfigured in real time. We also investigate the SER of an emitter located in the vicinity of the proposed MTS platform, demonstrating that the transition between metasurface topologies entails a dramatic increase of the local density of states (LDOS).

Consider an infinitesimally thin uniaxial metasurface in free-space defined by the conductivity tensor

$$\bar{\sigma} = \begin{pmatrix} \sigma_{xx} & 0 \\ 0 & \sigma_{yy} \end{pmatrix}. \quad (1)$$

Contrary to the case of isotropic surfaces, which support either transverse-magnetic (TM) or transverse-electric (TE) modes [19] (for  $\text{Im}[\sigma] > 0$  and  $\text{Im}[\sigma] < 0$ , respectively, where  $\sigma$  is the surface conductivity and an  $e^{i\omega t}$  time convention is assumed), uniaxial metasurfaces can simultaneously support the propagation of TE and TM surface plasmons [26–28]. TE modes are barely confined to the surface, thus being of little practical interest to enhance light-matter interactions. We focus here on highly confined TM modes, whose dispersion relation can be compactly written as [26–28]

$$\eta_0^2(k_x^2\sigma_{xx} + k_y^2\sigma_{yy})^2(k_x^2 + k_y^2 - k_0^2) - 4k_0^2(k_x^2 + k_y^2)^2 = 0. \quad (2)$$

This equation interestingly predicts different topologies for surface plasmon propagation as a function of the  $\bar{\sigma}$  components. *Elliptic* isotropic and anisotropic topologies arise when both conductivity components have a positive imaginary part, i.e.,  $\text{Im}[\sigma_{xx}] > 0$  and  $\text{Im}[\sigma_{yy}] > 0$ , thus leading to inductive surfaces that can support plasmon propagation. Energy in this case is mostly focused towards the direction with a lower imaginary conductivity component. A uniform graphene sheet, which possesses  $\text{Im}[\sigma_{xx}] = \text{Im}[\sigma_{yy}] > 0$  at terahertz and near infrared frequencies, is a natural example of elliptic isotropic topology. *Hyperbolic* dispersion topologies arise when the surface behaves as a dielectric (capacitive, with  $\text{Im}[\sigma] < 0$ ) along one direction, and as a metal (inductive, with  $\text{Im}[\sigma] > 0$ ) along the orthogonal one; i.e., they require that  $\text{sgn}(\text{Im}[\sigma_{xx}]) \neq \text{sgn}(\text{Im}[\sigma_{yy}])$ . In this scenario, Eq. (2) follows a hyperbolic surface whose branches are asymptotically approximated by [29]

$$k_y = \pm m k_x \pm b, \quad \text{with} \quad m = \sqrt{-\frac{\sigma_{xx}}{\sigma_{yy}}} \quad \text{and} \quad b = k_0 \sqrt{1 + \left(\frac{2}{\eta_0 \sigma_{yy}}\right)^2}, \quad (3)$$

revealing that the propagating plasmons can become extremely—ideally infinitely—confined along specific directions in space, both in the longitudinal [ $k_\rho(\varphi) \rightarrow \infty$ , being  $\varphi$  the angle of propagation within the surface] and in the transverse ( $\text{Im}[k_z] \rightarrow 0^+$ ) planes. As a special transition point of interest, the *extremely anisotropic  $\sigma$ -near-zero* scenario requires that one of the metasurface conductivity components presents a relatively small imaginary part compared to the

other one, i.e.,  $|\text{Im}[\sigma_{xx}]| \gg |\text{Im}[\sigma_{yy}]|$  or  $|\text{Im}[\sigma_{xx}]| \ll |\text{Im}[\sigma_{yy}]|$ , supporting the canalization regime originally studied in Ref. [25] for hyperlensing.

In order to illustrate the aforementioned concepts, Fig. 1 shows the distribution of electric field  $E_z$  normal to the surface induced by a  $z$ -oriented dipole located above various metasurfaces. In the isotropic elliptical case [Fig. 1(a),  $\text{Im}[\sigma_{xx}] = \text{Im}[\sigma_{yy}]$ ] the SPPs equally propagate in all directions along the surface, while in the anisotropic  $\sigma$ -near-zero metasurface [Fig. 1(b),  $\text{Im}[\sigma_{xx}] \gg \text{Im}[\sigma_{yy}]$ ] energy is strongly confined along a single direction ( $y$  axis). Figures 1(c)–1(d) show two different hyperbolic metasurfaces, illustrating how the supported plasmons travel towards the specific directions defined by the asymptotes of the hyperbolic dispersion relation. These directions can be easily determined—with respect to the  $x$  axis—by  $\varphi \approx \tan^{-1}[\pm\sqrt{-(\sigma_{xx}/\sigma_{yy})}]$ , confirming that an adequate tailoring of the MTS conductivity tensor allows a simple and powerful control of the SPP confinement and propagation direction [29]. Interestingly, the different metasurface topologies investigated here translate onto a 2D surface the unusual optical interaction offered in the bulk by HMTMs [4]. Although analogous, these scenarios are not dual of each other: the reduced dimensionality of metasurfaces imposes constraints to electromagnetic wave propagation—including the requirement to lie below the light cone—and leads to a rich new variety of phenomena and functionalities.

An array of densely packed graphene strips [see the inset of Fig. 2(a)] can implement the ideal platform to realize

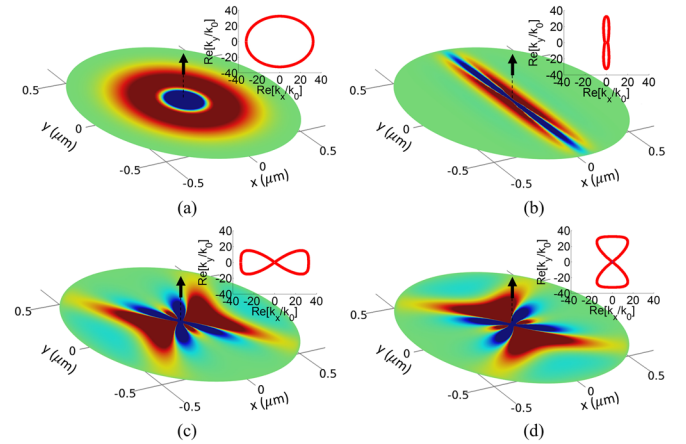


FIG. 1 (color online). SPP excitation along homogeneous uniaxial metasurfaces by a  $z$ -oriented dipole emitter (represented by a black arrow) located at a distance  $d = 10$  nm above the surface. The 2D plots show the  $E_z$  field component of propagating SPPs. The insets present the corresponding isofrequency contour. (a) Isotropic metasurface  $\sigma_{xx} = \sigma_{yy} = 0.08 + i0.1$  mS. (b) Extremely anisotropic  $\sigma$ -near-zero metasurface,  $\sigma_{xx} = 0.08 + i10$  mS,  $\sigma_{yy} = 0.08 - i0.1$  mS. (c) Hyperbolic metasurface,  $\sigma_{xx} = 0.08 - i0.1$  mS,  $\sigma_{yy} = 0.08 + i0.1$  mS. (d) Hyperbolic metasurface,  $\sigma_{xx} = 0.08 + i0.1$  mS,  $\sigma_{yy} = 0.08 - i0.1$  mS. Operation frequency is 10 THz.

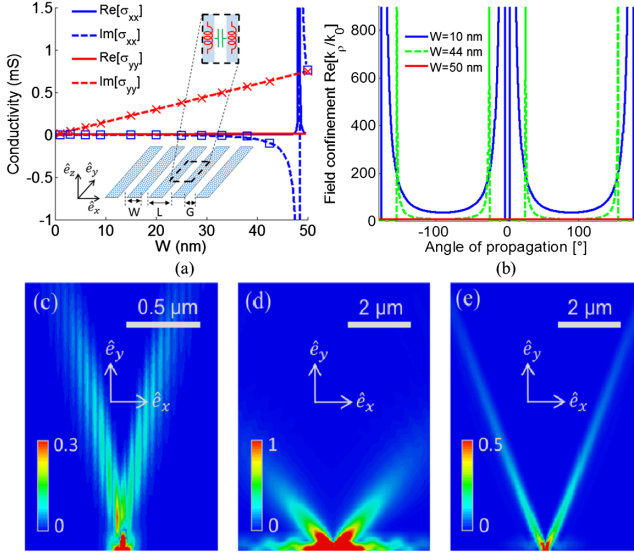


FIG. 2 (color online). Practical implementation of different metasurface topologies using an array of graphene strips. (a) Effective conductivity tensor of the uniaxial metasurface versus the strips width ( $W$ ) for a fixed period  $L = 50$  nm. Graphene chemical potential is  $\mu_c = 0.4$  eV. The inset shows a schematic of the proposed hyperbolic metasurface. Results have been computed with Eq. (4) (solid line) and are validated using a mode-matching approach (markers) [40]. (b) Field confinement of surface plasmons supported by the metasurface versus their angle of propagation with respect to the  $x$  axis. (c)–(e) Average power flow of SPPs excited on the structure (periodicity  $L = 50$  nm) by a  $z$ -oriented dipole located at 50 nm above the structure. The emitter is placed at the center bottom of the panels. (c)  $W = 10$  nm and graphene chemical potential  $\mu_c = 0.5$  eV. (d)–(e)  $W = 25$  nm and graphene chemical potential is set to (d)  $\mu_c = 0.1$  eV and (e)  $\mu_c = 0.3$  eV. Operation frequency is 10 THz.

the aforementioned metasurface topologies at terahertz and near infrared frequencies. While this geometry was previously considered in the literature for different purposes (see Refs. [18] and [39,40]), its in-plane nature offers unusual and exciting possibilities. Importantly, it provides significant advantages compared to previous attempts to implement anisotropic  $\sigma$ -near-zero metasurfaces [17], [25], such as the possibility of realizing any topology of interest, a simple control of the MTS conductivity tensor by adjusting the surface geometry or its electrical bias, feasible fabrication using  $e$ -beam lithography, inherent broadband nature, and powerful electrical reconfiguration. The in-plane effective conductivity tensor  $\bar{\sigma}^{\text{eff}}$  of the proposed structure can be analytically obtained using an effective medium theory as

$$\sigma_{yy}^{\text{eff}} = \sigma \frac{W}{L} \quad \text{and} \quad \sigma_{xx}^{\text{eff}} = \frac{L\sigma\sigma_C}{W\sigma_C + G\sigma}, \quad (4)$$

where  $L$  and  $W$  are the periodicity and width of the strips, respectively,  $G$  is the separation distance between two consecutive ribbons,  $\sigma$  is graphene conductivity and  $\sigma_C = -j(\omega\epsilon_0 L/\pi) \ln[\csc(\pi G/2L)]$  is an equivalent

conductivity associated with the near-field coupling between adjacent strips obtained using an electrostatic approach [41]. This theory is valid when the homogeneity condition  $L \ll \lambda_{\text{SPP}_x}$  is satisfied, being  $\lambda_{\text{SPP}_x}$  the plasmon wavelength in the direction perpendicular to the strips ( $x$  in this case), thus leading to homogeneous 2D metasurfaces. The topology of the proposed structure may range from elliptical to hyperbolic as a function of its geometrical parameters and graphene characteristics, as revealed in Eq. (4). In order to further investigate its behavior, Fig. 2(a) shows the different components of  $\bar{\sigma}^{\text{eff}}$  versus the strip width  $W$  for a fixed value of the period  $L = 50$  nm. Results have been computed using Eq. (4), and have been validated by a rigorous mode-matching numerical approach [40].  $\text{Im}[\sigma_{yy}^{\text{eff}}]$  is mainly governed by graphene (inductive,  $\text{Im}[\sigma] > 0$ ), thus providing a plasmonlike response to the surface.  $\text{Im}[\sigma_{xx}^{\text{eff}}]$ , on the other hand, is directly proportional to the near-field coupling between strips (capacitive,  $\text{Im}[\sigma_C] < 0$ ), which provides the desired dielectriclike behavior. In addition,  $\text{Im}[\sigma_{xx}^{\text{eff}}]$  resonates at the condition  $G\text{Im}[\sigma] + W\text{Im}[\sigma_C] = 0$ , which divides the metasurface response in two clear regions as a function of the strip width. For widths  $W > -G\text{Im}[\sigma/\sigma_C]$ , the array of strips behaves as an elliptic anisotropic metasurface (with  $\text{Im}[\sigma_{yy}^{\text{eff}}] > 0$  and  $\text{Im}[\sigma_{xx}^{\text{eff}}] > 0$ ), evolving into an isotropic ( $\text{Im}[\sigma_{yy}^{\text{eff}}] = \text{Im}[\sigma_{xx}^{\text{eff}}]$ ) surface as  $G \rightarrow 0$ . However, for  $W < -G\text{Im}[\sigma/\sigma_C]$ ,  $\text{Im}[\sigma_{xx}^{\text{eff}}]$  is always negative, therefore leading to HMTSSs. In this region,  $\text{Im}[\sigma_{xx}^{\text{eff}}]$  may provide a wide variety of values, thus allowing the implementation of HMTSSs supporting plasmons that travel towards any desired direction [29]. This general behavior of  $\bar{\sigma}^{\text{eff}}$  is maintained for different values of the period  $L$ . Different values of graphene chemical potential  $\mu_c$ , which may be tuned in practice by applying a gate voltage [22], allow controlling the properties of  $\bar{\sigma}^{\text{eff}}$ , thus leading to the possibility of electrically reconfiguring the MTS topology [29]. Figure 2(b) shows the field confinement of surface plasmons supported by some implementations of the proposed structure versus their propagation angle within the metasurface. Our results demonstrate that hyperbolic plasmons can achieve extremely large field confinement in some specific directions, while retaining similar loss level than plasmons in isotropic unpatterned graphene [29]. For instance, field confinement values larger than  $200k_0\lambda_{\text{SPP}} \leq 5 \times 10^{-3}\lambda_0$ —can be achieved with a slight increase, around 4.5%, in absorption. Even though this study considers high-quality graphene [30], these conclusions are independent of graphene losses [29]. Finally, Figs. 2(c)–2(e) show the distribution of the electric field magnitude for surface plasmons excited by a  $z$ -oriented dipole and propagating along a realistic array of graphene strips with different hyperbolic dispersion controlled by the applied chemical potential, demonstrating the ability of the proposed platform to support extremely confined SPPs and electrically control their propagation. It is important to point out that the SPPs

supported by this hyperbolic MTS are not ideally confined up to infinite wave vector numbers, as implied by Eq. (3). Field confinement and the maximum guided wave number are inherently limited in practice by two factors: (i) the presence of losses, which closes the otherwise open isofrequency contours [29], and (ii) the granularity of the metasurface, which, when comparable to the SPP wavelength, invalidates the homogenization model. This implies that for low-loss graphene strip arrays the upper cutoff to SPP propagation is given by  $\lambda_{\text{SPP}_x} \sim L/2$ , which for the values considered in Fig. 2(b) limits the maximum field confinement to values below  $1200k_0$ .

The SER of an arbitrarily oriented dipole (i.e., a quantum dot or an excited molecule) located above the proposed metasurface offers remarkable possibilities. The analogy with emitter interactions with HMTMs [2,9] suggests that the local density of states should be boosted by HMTS, given the unbounded nature of the supported plasmon spectrum, but the different underlying physics requires a careful analysis. For this purpose, the emitter SER was computed using a dedicated Green's function approach [42], [43], and Fig. 3(a) shows the calculated SER for a  $z$ -oriented dipole placed 5 nm above a lossless homogeneous metasurface whose conductivity tensor components are simultaneously varied, implementing all possible metasurface topologies. In the elliptic region [first quadrant of Fig. 3(a), with  $\text{Im}[\sigma_{xx}] > 0$  and  $\text{Im}[\sigma_{yy}] > 0$ ], the in-plane wave number of the supported SPPs decreases as long as the conductivity components increase [Fig. 3(b)], producing low-confined plasmons unable to couple energy from incoming evanescent waves with large wave numbers. The corresponding SER values are small. The third quadrant of Fig. 3(a) ( $\text{Im}[\sigma_{xx}] < 0$  and  $\text{Im}[\sigma_{yy}] < 0$ ) also implements an elliptic topology, for which SER is even lower since the corresponding surface supports barely confined TE plasmons with negligible near-field interactions. Hyperbolic topologies are found in the second ( $\text{Im}[\sigma_{xx}] > 0$ ,  $\text{Im}[\sigma_{yy}] < 0$ ) and fourth ( $\text{Im}[\sigma_{xx}] < 0$ ,  $\text{Im}[\sigma_{yy}] > 0$ ) quadrants, and they provide a significant SER increase—between 2 and 4 orders of magnitude. The calculated SER value is still finite, due to the finite, albeit small, distance of the emitter from the surface. Interestingly, the SER decreases for increasing absolute values of the conductivity components. This is due to the progressive shift of the hyperbolic branches as the conductivity increases [see Eq. (2) and Fig. 3(c)], which in turn prevents the coupling of waves with low wave numbers to the MTS, and, therefore, decreases the overall local density of states. The inset of Fig. 3(a) highlights the topological transition between elliptic and hyperbolic topologies, i.e., the extreme anisotropic  $\sigma$ -near-zero case. In this scenario, the emitter SER is further increased thanks to the flattening of the metasurface isofrequency contour that allows the structure to simultaneously couple incoming waves with low and high wave numbers, in analogy to that found in bulk

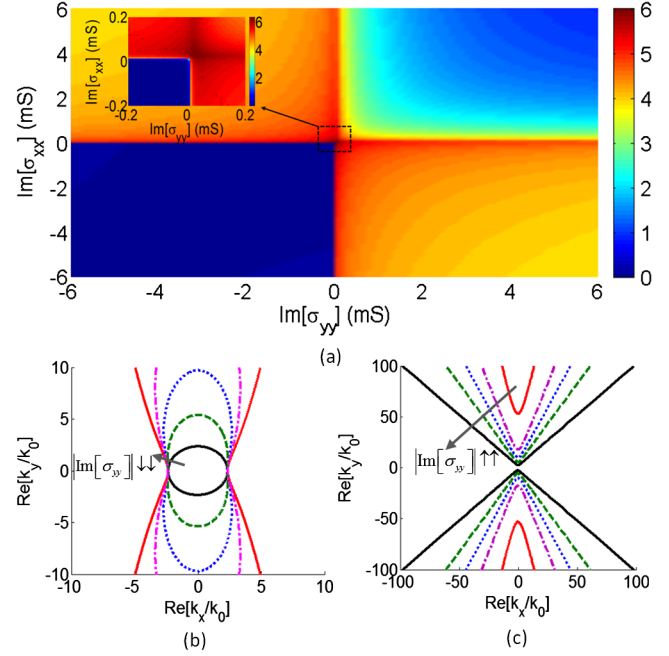


FIG. 3 (color online). Topological transitions in metasurfaces. (a) SER in logarithm scale of a  $z$ -oriented dipole located at  $d = 5$  nm above a lossless uniaxial metasurface. The conductivity components of the structure are simultaneously varied in order to fully explore the SER in all topologies, including elliptic (first and third quadrants) and hyperbolic (second and fourth quadrants) cases. The inset details the transition among all topologies. (b) Lossless elliptic isofrequency contours, ranging from the isotropic case ( $\text{Im}[\sigma_{xx}] = \text{Im}[\sigma_{yy}] = 2.5$  mS, black solid line) to the extremely anisotropic  $\sigma$ -near-zero case ( $\text{Im}[\sigma_{xx}] = 2.5$ ,  $\text{Im}[\sigma_{yy}] = 0.005$  mS, red solid line). (c) Lossless hyperbolic isofrequency contours, ranging from the isotropic case ( $\text{Im}[\sigma_{xx}] = -2.5$ ,  $\text{Im}[\sigma_{yy}] = 2.5$  mS, black solid line) to the extremely anisotropic  $\sigma$ -near-zero case ( $\text{Im}[\sigma_{xx}] = -2.5$ ,  $\text{Im}[\sigma_{yy}] = 0.1$  mS, red solid line). Operation frequency is 10 THz.

HMTMs [9,44]. In the case of elliptic anisotropic  $\sigma$ -near-zero metasurfaces, this flattening allows the surface to interact with evanescent waves with large wave numbers, while for HMTSs the flattening permits the coupling of incoming waves with low wave numbers, which were previously mismatched due to the rounded shape of the hyperbolic dispersion relation. The fundamental advantage of these hyperbolic surface responses compared to HMTMs resides in the possibility of funneling the radiated energy within the surface, where it may be easily accessed with near-field techniques, processed, and radiated out using in-plane gratings or nanoantennas. Additional considerations on the robustness of this phenomenon to emitter orientation and to dissipation losses are detailed in Ref. [29].

Figure 4 demonstrates that the SER strongly depends on the separation distance between emitter and surface. In the limit of a radiating dipole sitting on lossless, homogeneous HMTSs, the LDOS goes to infinity. In this ideal scenario, the emitter would provide an infinite amount of energy,

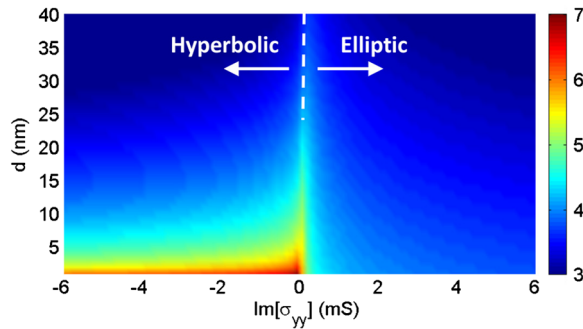


FIG. 4 (color online). SER of a  $z$ -oriented dipole located above a lossless uniaxial metasurface. The 2D plot shows the Purcell enhancement in logarithmic scale versus (i) the distance of the dipole from the metasurface, and (ii) different  $\sigma_{yy}$  values, considering a fix  $\sigma_{xx} = i0.2$  mS conductivity component. Operation frequency is 10 THz.

able to excite an unbounded set of surface plasmons ( $\lambda_{\text{SPP}} \rightarrow 0$ ) propagating on the surface. In practice, the presence of losses and the finite granularity of the engineered metasurface limits the LDOS blowup, as expected. When the emitter is at a finite distance ( $\sim \text{nm}$ ) above the surface, the SER can become several orders of magnitude larger in the hyperbolic regime than in the elliptic one, with most of the radiated energy coupled along the metasurface. As the separation distance between emitter and MTS increases, due to the attenuation of the evanescent spectrum in free space, the local density of states decreases and, at a critical distance, the SER may become higher in the elliptical than in the hyperbolic regime, indicating that the energy coupled into SPPs is mainly carried by waves with reduced wave numbers.

In conclusion, we have proposed the concept of ultrathin reconfigurable hyperbolic and  $\sigma$ -near-zero metasurfaces, describing the properties of the supported plasmons and the large enhancement of light-matter interactions they may provide. An array of densely packed graphene strips has been proposed as a possible physical implementation of these metasurfaces. The structure, which is elegantly described by an in-plane effective impedance, provides interesting advantages, such as a simple control of the uniaxial metasurface conductivity tensor components by simple geometrical parameters, ability to implement any MTS topology, and real-time electrical reconfigurability. The proposed metasurfaces may lead to a new class of planarized plasmonic devices able to strongly interact with the incoming light, allowing extreme confinement, easy access, processing, and radiation in dynamically reconfigurable directions.

This work was supported by the Air Force Office of Scientific Research Grant No. FA9550-13-1-0204, the Welch foundation with Grant No. F-1802, and the National Science Foundation with Grant No. ECCS-1406235.

\*alu@mail.utexas.edu

- [1] D. R. Smith and D. Schurig, *Phys. Rev. Lett.* **90**, 077405 (2003).
- [2] H. N. S. Krishnamoorthy, Z. Jacob, E. Narimanov, I. Kretzschmar, and V. M. Menon, *Science* **336**, 205 (2012).
- [3] A. Poddubny, I. Iorsh, P. Belov, and Y. Kivshar, *Nat. Photonics* **7**, 948 (2013).
- [4] V. P. Drachev, V. A. Podolskiy, and A. V. Kildishev, *Optic. Express* **21**, 15048 (2013).
- [5] N. Engheta and R. Ziolkowski, *Metamaterials: Physics and Engineering Explorations* (Wiley, New York, 2006).
- [6] C. Argyropoulos, N. M. Estakhri, F. Monticone, and A. Alù, *Optic. Express* **21**, 15037 (2013).
- [7] A. V. Chshelokova, P. V. Kapitanova, A. N. Poddubny, D. S. Filonov, A. P. Slobzhanyuk, Yu. S. Kivshar, and P. A. Belov, *J. Appl. Phys.* **112**, 073116 (2012).
- [8] M. A. K. Othman, C. Guclu, and F. Capolino, *Opt. Express* **21**, 7614 (2013).
- [9] A. N. Poddubny, P. A. Belov, and Y. S. Kivshar, *Phys. Rev. A* **84**, 023807 (2011).
- [10] D. Lu, J. J. Kan, E. E. Fullerton, and Z. Liu, *Nat. Nanotechnol.* **9**, 48 (2014).
- [11] Z. Jacob, L. V. Alekseyev, and E. Narimanov, *Opt. Express* **14**, 8247 (2006).
- [12] A. Salandrino and N. Engheta, *Phys. Rev. B* **74**, 075103 (2006).
- [13] N. Yu and F. Capasso, *Nat. Mater.* **13**, 139 (2014).
- [14] A. V. Kildishev, A. Boltasseva, and V. M. Shalae, *Science* **339**, 1232009 (2013).
- [15] F. Monticone, N. M. Estakhri, and A. Alù, *Phys. Rev. Lett.* **110**, 203903 (2013).
- [16] A. V. Shchelokova, D. S. Filonov, P. V. Kapitanova, and P. A. Belov, *Phys. Rev. B* **90**, 115155 (2014).
- [17] Y. Liu and X. Zhang, *Appl. Phys. Lett.* **103**, 141101 (2013).
- [18] F. H. L. Koppens, D. E. Chang, and F. J. García de Abajo, *Nano Lett.* **11**, 3370 (2011).
- [19] G. W. Hanson, *J. Appl. Phys.* **103**, 064302 (2008).
- [20] F. Javier García de Abajo, *ACS Photonics* **1**, 135 (2014).
- [21] J. S. Gómez-Díaz and J. Perruisseau-Carrier, *Opt. Express* **21**, 15490 (2013).
- [22] J. S. Gómez-Díaz, M. Esquis-Morote, and J. Perruisseau-Carrier, *Opt. Express* **21**, 24856 (2013).
- [23] P. Chen, H. Huang, D. Akinwande, and A. Alù, *ACS Photonics* **1**, 647 (2014).
- [24] D. L. Sounas, H. S. Skulason, H. V. Nguyen, A. Guermoune, M. Sij, T. Szkopek, and C. Caloz, *Appl. Phys. Lett.* **102**, 191901 (2013).
- [25] E. Forati, G. W. Hanson, A. B. Yakovlev, and A. Alù, *Phys. Rev. B* **89**, 081410 (2014).
- [26] H. J. Bilow, *IEEE Trans. Antennas Propag.* **51**, 2788 (2003).
- [27] A. M. Patel and A. Grbic, *IEEE Trans. Antennas Propag.* **61**, 211 (2013).
- [28] R. Quarfoth and D. Sievenpiper, *IEEE Trans. Antennas Propag.* **61**, 3597 (2013).
- [29] See Supplemental Material at <http://link.aps.org/supplemental/10.1103/PhysRevLett.114.233901>, which includes Refs. [30–38], for a detailed discussion of the asymptotic behavior of HMTS, and additional considerations related to the SER of an arbitrarily oriented emitter located above lossy HMTSs. Further analysis regarding the

- features of hyperbolic plasmons supported by an array of graphene strips versus graphene quality are also provided.
- [30] G. W. Hanson, A. B. Yakovlev, and A. Mafi, *J. Appl. Phys.* **110**, 114305 (2011).
- [31] N. -A. P. Nicorovici, R. C. McPhedran, and L. C. Botten, *Physica B (Amsterdam)* **405**, 2915 (2010).
- [32] O. Di Stefano, N. Fina, S. Savasta, R. Girlanda, and M. Pieruccini, *J. Phys. Condens. Matter* **22**, 315302 (2010).
- [33] C. T. Tai, L. Fellow, and R. E. Collin, *IEEE Trans. Antennas Propag.* **48**, 1501 (2000).
- [34] P. Tassin, T. Koschny, and C. M. Soukoulis, *Science* **341**, 620 (2013).
- [35] Y. R. Padooru, A. B. Yakovlev, C. S. R. Kaipa, G. W. Hanson, F. Medina, and F. Mesa, *Phys. Rev. B* **87**, 115401 (2013).
- [36] C. Dean, A. Young, I. Meric, C. Lee, L. Wang, S. Sorgenfrei, K. Watanabe, T. Taniguchi, P. Kim, K. Shepard *et al.*, *Nat. Nanotechnol.* **5**, 722 (2010).
- [37] [www.comsol.com](http://www.comsol.com).
- [38] [www.cst.com](http://www.cst.com).
- [39] O. V. Shapoval, J. S. Gomez-Diaz, J. Perruisseau-Carrier, J. R. Mosig, and A. I. Nosich, *IEEE Trans. Terahertz Sci. Technol.* **3**, 666 (2013).
- [40] M. Tymchenko, A. Y. Nikitin, and L. Martín-Moreno, *ACS Nano* **7**, 9780 (2013).
- [41] C. S. R. Kaipa, A. B. Yakovlev, G. W. Hanson, Y. R. Padooru, F. Medina, and F. Mesa, *Phys. Rev. B* **85**, 245407 (2012).
- [42] A. Lakhtakia, *Int. J. Infrared Millim. Waves* **13**, 161 (1992).
- [43] L. Novotny and B. Hecht, *Principles of Nano-Optics* (Cambridge University Press, Cambridge, England, 2006).
- [44] A. V. Chebykin, A. A. Orlov, A. S. Shalin, A. N. Poddubny, and P. A. Belov, *Phys. Rev. B* **91**, 205126 (2015).